Self-sustaining vortex perturbations in smooth shear flows

J.-H. Kim, J. C. Perez, and W. Horton
Institute for Fusion Studies, The University of Texas at Austin, Austin, Texas 78712

G. D. Chagelishvili, R. G. Changishvili, and J. G. Lominadze
Abastumani Astrophysical Observatory, A. Kazbegi 2a, Tbilisi 0160, Georgia

John C. Bowman
*Department of Mathematical and Statistical Sciences, University of Alberta,
Edmonton, Alberta, Canada, T6G 2G1*

The nonlinear dynamics of coherent circular/elliptical cyclonic and anticyclonic vortices in plane flow with constant shear is investigated numerically using a dealiased Fourier pseudospectral code. The flow is asymptotically linearly stable, but is highly non-normal, allowing perturbations to gain energy transiently from the background shear flow. This linear transient growth interplays with nonlinear processes. In certain cases it is shown that the nonlinear feedback is positive, leading to self-sustaining coherent vortices. Self-sustaining coherent vortices exist where the vorticity is parallel to the mean flow vorticity (cyclonic rotation). The required nonlinear feedback is absent for small amplitude anticyclonic vortices. However, elliptical anticyclonic vortices become self-sustaining if the amplitude exceeds a threshold value. The self-sustaining of coherent vortices is similar to the subcritical, so-called bypass, transition to turbulence in shear flows. The common features are: transient linear growth; positive nonlinear feedback; and anisotropy of the linear and nonlinear phenomena (in contrast to isotropic Kolmogorov turbulence). A plasma laboratory experiment is suggested based on the results of this investigation. © *2006 American Institute of Physics*. [DOI: 10.1063/1.2209229]

I. INTRODUCTION

A turning point in understanding the energy-intensive processes having their kinematic origin in smooth (inflection-free) shear flows that are stable according to the Rayleigh criterion has already been reached.[1] The understanding came from recognizing the deficiency of the modal approach (spectral expansion of perturbations in time and analysis of the eigenmodes) for shear flows. The linear operators in the mathematical formalism of the modal analysis of shear flows (e.g., plane Couette and plane Poiseuille flows) are non-normal and the corresponding eigenmodes are nonorthogonal and strongly interfere.

A correct approach analyzes the interference of the eigenmodes. In modal analysis, the focus is on the asymptotic stability of flows, whereas little attention is directed to any particular initial value or finite time period of the dynamics. The transient evolution is regarded as having no significance and left for speculation.

However, in the 1990s, the emphasis shifted from the analysis of long-time asymptotic flow stability to the study of transient behavior. The transient analyses have demonstrated linear transient growth of asymptotically stable hydrodynamic flows.[2–5]

It was suggested that transient linear growth modifies the asymptotic behavior of the system if the nonlinearity plays a role.[6,7] The modification of asymptotic behavior by transient growth leads to the concept of the onset of turbulence in spectrally stable shear flows, the so-called *bypass transition*.[4,5,7–13]

In the bypass transition, small perturbations become large enough by the transient growth that nonlinear interaction plays a role. The nonlinear terms are conservative and can only redistribute fluctuation energy among the modes. In the presence of sufficiently strong shear flow, energy can be redistributed in a way that reinforces the linear transient growth. A series of phenomena closes the loop so that the growth phase can persist. This function of the nonlinearity is coined "nonlinear mixing"[6,7] or "positive nonlinear feedback".[13] Hereafter, we use the term positive nonlinear feedback, as this clearly underscores the positive action of loop nonlinearities.

In a simple shear flow obeying the Euler equation (analogous to the Hasegawa–Mima[14] equation in plasma physics), we will demonstrate (1) the transient growth of vortical perturbations, (2) the evidence for positive nonlinear feedback, and (3) the simultaneous interaction of these linear and nonlinear processes required for the perturbation to be self-sustaining. In Sec. II, we introduce all necessary definitions and equations. In Sec. III, we numerically illustrate the previous three issues regarding the dynamics of coherent vortical perturbations in an unbounded flow with a linear velocity shear. Perturbations in turbulent flows are chaotic, but the self-sustenance scenarios for chaotic and coherent perturbations are similar. Furthermore, coherent vortices may be the main product of the dynamics and play a determining role in anomalous transport phenomena.[15,16] In Sec. IV, a simple sketch of the self-sustenance of perturbations in the wave number plane is presented. We compare the turbulence scenarios in spectrally stable and unstable flow systems. The scenarios illustrate the principal differences in the spectral

13, 062304-1

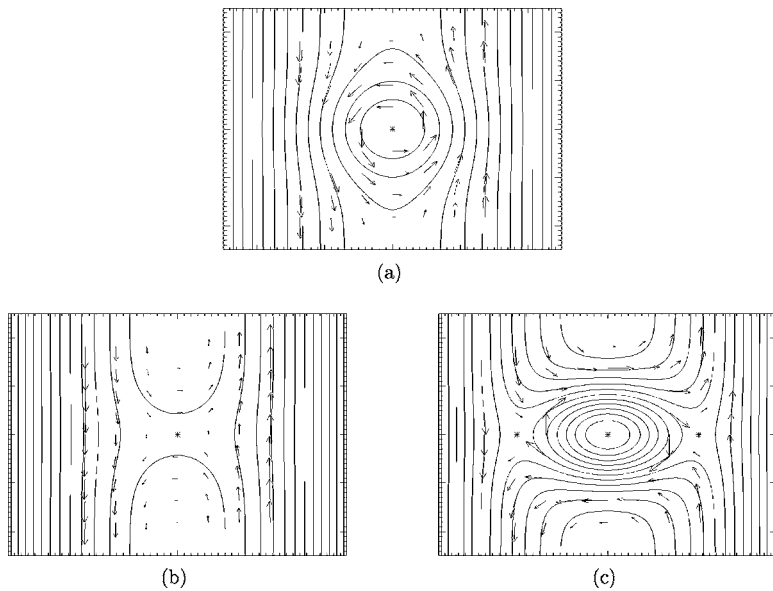FIG. 1. The flow diagram of the background flow with (a) cyclonic vortex ($B < 0$), (b) anticyclonic vortex with one stagnation point ($0 < B < 0.5$), and (c) anticyclonic vortex with three stagnation points ($B > 0.5$). The asterisks (*) indicate stagnation points.

characteristics of these turbulent regimes. In Sec. VI, a laboratory plasma experiment is suggested based on the results of this investigation. Some concluding remarks are presented in Sec. VII.

II. BASIC EQUATIONS AND PROCESSES

The interplay of linear transient and nonlinear feedback phenomena can be understood on the basis of the following two-dimensional hydrodynamic equation:

$$\left[\frac{\partial}{\partial t} + U_0(x)\frac{\partial}{\partial y}\right]\Delta\psi + J(\psi, \Delta\psi) - \nu\Delta^2\psi = 0, \qquad (1)$$

where ψ is the stream function of a perturbation and ν is the kinematic viscosity. The spatial operators J and Δ represent the two-dimensional Jacobian and Laplacian, respectively. The basic flow velocity $\mathbf{U}_0(x) = (0, Ax)$ has a positive constant shear A in the x direction. The velocity $\mathbf{v}$, the vorticity $\boldsymbol{\omega}$ and energy density e of the perturbation are defined in terms of the stream function ψ and the constant fluid mass density ρ:

$$\mathbf{v} = (v_x, v_y) = \hat{\mathbf{z}} \times \boldsymbol{\nabla}\psi = \left(-\frac{\partial\psi}{\partial y}, \frac{\partial\psi}{\partial x}\right), \qquad (2)$$

$$\boldsymbol{\omega} = \boldsymbol{\nabla} \times \mathbf{v} = \left(\frac{\partial v_y}{\partial x} - \frac{\partial v_x}{\partial y}\right)\hat{\mathbf{z}} = \Delta\psi\hat{\mathbf{z}}, \qquad (3)$$

$$e(x,y,t) = \frac{1}{2}\rho\left[\left(\frac{\partial\psi}{\partial x}\right)^2 + \left(\frac{\partial\psi}{\partial y}\right)^2\right]. \qquad (4)$$

The vorticity $\boldsymbol{\omega}$ measures the local angular momentum per unit mass of the fluid and the Jacobian operator describes the Lie or convective derivative $\mathbf{v}\cdot\boldsymbol{\nabla}\boldsymbol{\omega}$ of the vorticity.

In this work we study cyclonic and anticyclonic coherent vortical perturbations linearly and nonlinearly. Cyclonic vortices are parallel to the basic flow vorticity $\boldsymbol{\nabla} \times \mathbf{U}_0 = A\hat{\mathbf{z}}$.

Anticyclonic vortices are antiparallel to the basic flow vorticity. A generic form for vortical perturbations in the (x, y) plane is the local Gaussian stream function

$$\psi_0 \equiv \psi(x,y,t)\Big|_{t=0} = b\exp\left(-\frac{x^2 + \alpha^2 y^2}{\ell^2}\right), \qquad (5)$$

where α characterizes the eccentricity of the initial coherent vortex and ℓ characterizes the vortex size.

We introduce dimensionless variables using the time scale A^{-1} of the background shear flow vorticity and the spatial scale ℓ. The nondimensional parameters are

$$\tau \equiv At, \quad X \equiv \frac{x}{\ell}, \quad Y \equiv \frac{y}{\ell}, \quad B \equiv \frac{b}{A\ell^2}, \quad \Psi \equiv \frac{\psi}{A\ell^2},$$

$$V_x = \frac{v_x}{A\ell}, \quad V_y = \frac{v_x}{A\ell}, \quad E \equiv \frac{2e}{\rho A^2\ell^2}, \quad R_e \equiv \frac{A\ell^2}{\nu}.$$

In the dimensionless variables the dynamical Eq. (1) becomes

$$\left(\frac{\partial}{\partial\tau} + X\frac{\partial}{\partial Y}\right)\Delta\Psi + J(\Psi, \Delta\Psi) - R_e^{-1}\Delta^2\Psi = 0, \qquad (6)$$

with the dimensionless energy density

$$E(\tau) = \left(\frac{\partial\Psi}{\partial X}\right)^2 + \left(\frac{\partial\Psi}{\partial Y}\right)^2 \qquad (7)$$

and the dimensionless initial vortex function

$$\Psi\big|_{\tau=0} = B\exp(-X^2 - \alpha^2 Y^2). \qquad (8)$$

The shear parameter A, the amplitude of the initial perturbation b, and the characteristic linear scale along the flow ℓ combine to form one parameter B, which represents the defining parameter of the vortex dynamics. The parameter B is the ratio of the vortex eddy turnover time to the shear time scale. Large values of B represent strong nonlinear interaction compared to the linear shear interaction. As shown in Fig. 1(a), coherent vortices with a negative value of B have

the same sign as the basic flow vorticity (counterclockwise flow) and are cyclonic. The vortices with a positive value of B have the opposite sign (clockwise flow) relative to the basic flow vorticity and represent anticyclonic vortices. For an anticyclonic vortex, there are stagnation points in the flow between the outer sheared flow and the inner vortex flow. For small amplitude anticyclonic vortices ($0 < B < 0.5$) in Fig. 1(b), there exists one stagnation point, whereas for large amplitude anticyclonic vortices ($B > 0.5$) in Fig. 1(c), there exist three stagnation points. These different configurations of the flow diagrams result in the different dynamics of the coherent anticyclonic vortices. Especially, as one will see later, the threshold $B = b/A\ell^2 \sim 0.5$ gives a reasonable estimate for the onset of total energy amplification for anticyclonic vortices.

On performing Fourier analysis with respect to the variables X and Y:

$$\Psi = \int dk_X dk_X \Psi_{\mathbf{k}} \exp(ik_X X + ik_X Y), \tag{9}$$

one finds

$$k^2 \frac{\partial \Psi_{\mathbf{k}}}{\partial \tau} - k_Y \frac{\partial (k^2 \Psi_{\mathbf{k}})}{\partial k_X} + R_e^{-1} k^4 \Psi_{\mathbf{k}}$$
$$= \sum_{\mathbf{k} = \mathbf{k}' + \mathbf{k}''} (k_X' k_Y'' - k_X'' k_Y') k'^2 \Psi_{\mathbf{k}'} \Psi_{\mathbf{k}''}, \tag{10}$$

$$E_{\mathbf{k}} = k^2 |\Psi_{\mathbf{k}}|^2, \tag{11}$$

where $k^2 \equiv k_X^2 + k_Y^2$ and $E_{\mathbf{k}}$ is twice the spectral energy density associated with the wave vector $\mathbf{k}$.

Equations (10) and (11) form the basis of our numerical study: with these equations, one can quantitatively explore the dynamics of the stream function, spectral energy density, and total perturbed energy. However, to investigate the physics of the phenomena, it is helpful to analyze the dynamical equation for the spectral energy density, which follows from Eqs. (10) and (11):

$$\frac{\partial E_{\mathbf{k}}}{\partial \tau} - \frac{2 k_X k_Y}{k^2} E_{\mathbf{k}} + \nabla_{\mathbf{k}} \cdot (V_k E_{\mathbf{k}}) + 2 R_e^{-1} k^2 E_{\mathbf{k}} = \hat{N}_{\mathbf{k}}, \tag{12}$$

where $\nabla_{\mathbf{k}} = (\partial/\partial k_X, \partial/\partial k_Y)$, $\mathbf{V}_k = (-k_Y, 0)$ and

$$\hat{N}_{\mathbf{k}} = \sum_{\mathbf{k} = \mathbf{k}' + \mathbf{k}''} (k_X' k_Y'' - k_X'' k_Y') k'^2 (\Psi_{\mathbf{k}}^* \Psi_{\mathbf{k}'} \Psi_{\mathbf{k}''} + \Psi_{\mathbf{k}} \Psi_{\mathbf{k}'}^* \Psi_{\mathbf{k}''}^*). \tag{13}$$

The term $\mathbf{V}_k E_{\mathbf{k}}$ represents the energy density flux in the wave number plane. The convolution in $\hat{N}_{\mathbf{k}}$ is a complicated function of $\Psi_{\mathbf{k}}$ that describes the effect of nonlinear interactions on the total energy change.

One can see from Eq. (12) that the dynamics of $E_{\mathbf{k}}$ is the result of the interplay of four basic phenomena:

(a)   The second term on the left-hand side (lhs) represents the energy exchange between the perturbations and the background flow. Spatial Fourier harmonics (SFHs) for which $k_X(\tau) k_Y > 0$ gain energy from the background flow and their amplitudes increase, whereas the amplitudes of SFHs for which $k_X(\tau) k_Y < 0$ decrease.

(b)   The third term on the lhs represents the linear "drift" of SFHs, $k_X(\tau) = k_X(0) - k_Y \tau$, in the wave number plane. The drift is caused by shearing of the perturbations by the background shear flow. Physically the linear drift corresponds to the statement that shear produces small-scale structures in the longtime limit. We see that the drift of a SFH does not cause a variation of the total energy of a perturbation ($\int dk_X dk_Y \nabla_{\mathbf{k}} \cdot (V_k E_{\mathbf{k}}) = 0$), but results in a transfer of SFHs from the amplification region ($k_X(\tau) k_Y > 0$) to the attenuation one ($k_X(\tau) k_Y < 0$). In terms of some characteristic wave number $k_0 = (k_{0X}, k_{0Y})$ of the energy spectrum, the time τ_{max} to reach the maximum energy and the maximum energy amplification ΔE_{max} can be approximated as

$$\tau_{max} \approx \frac{k_{0X}}{k_{0Y}}, \quad \Delta E_{max} \approx \left(1 + \frac{k_{0X}^2}{k_{0Y}^2}\right) E_0.$$

A large transient amplification $\Delta E_{max}/E_0 \gg 1$ occurs for the high k_{0X}/k_{0Y} modes in the region $k_{0X} k_{0Y} > 0$.

(c)   The fourth term on the lhs represents the energy dissipation by viscosity.

(d)   Nonlinear interactions in $\hat{N}_{\mathbf{k}}$ on the right-hand side (rhs) lead to energy exchange between different SFHs, redistributing perturbation energy on the wave number plane while leaving the total energy unchanged.

III. THE DYNAMICS OF COHERENT VORTICES—NUMERICAL SIMULATIONS

The simulations were done using the dealiased Fourier pseudospectral method, with a 256×256 grid superimposed on a spatial box of size $40\ell \times 40\ell$, yielding a minimum wave number $k_1 \ell$ of $2\pi/40 = 0.157$ and maximum wave number $k_{max}\ell = 85 k_1$.

In the simulations, we computed the total energy evolution of circular ($\alpha = 1$) vortices at $B = \pm 0.1$ to ± 11.0, $R_e = \infty$ (Fig. 2) and $R_e = 100$ (Fig. 3). The normalized total energy of the perturbations is given by

$$\frac{E(\tau)}{E(0)} \equiv \frac{\int dk_X dk_Y E_{\mathbf{k}}(\tau)}{\int dk_X dk_Y E_{\mathbf{k}}(0)}. \tag{14}$$

The simulations were also performed for elliptical vortices of two different aspect ratios, one extended ($\alpha = 1/2$) and one contracted ($\alpha = 2$) in the Y direction (Fig. 4). The values of B were chosen to get the same energy as in the circular case. The initial energies of the vortex with $\alpha = 1/2, 2$ and $B = \pm 4.472$ are equal to the initial energy of the circular vortex with $B = 5.0$. The results of the numerical simulations are presented in Figs. 2–5.

Figure 4 shows that the shape of the vortex is also critical. The energy of the streamwise cyclonic vortex drops steeply and then bounces up, but the final energy is still less than the initial energy.

A necessary condition for the self-sustenance of perturbations—in our case, for the self-sustenance of coherent circular/elliptical perturbations—is positive nonlinear
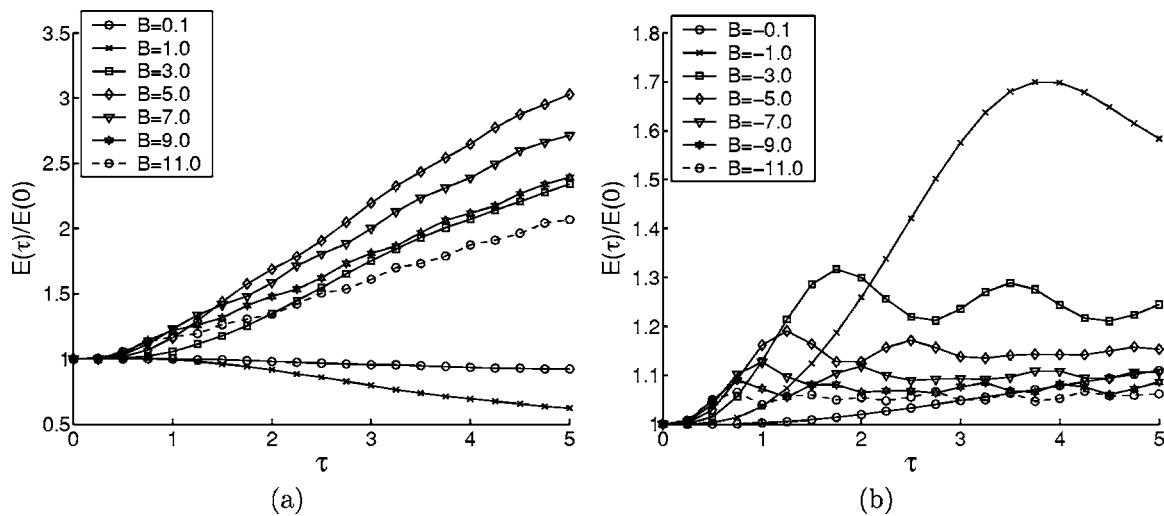
FIG. 2. Time evolutions of (a) anticyclonic and (b) cyclonic perturbation energies at $R_e = \infty$ plotted with different B values. The total perturbation energy is normalized by the initial energy.

feedback. The dominant transfer of Fourier harmonics by nonlinear processes must be from the attenuation domains (quadrants II and IV in **k** plane) to the amplification domains (quadrants I and III in **k** plane); i.e., one requires a predominantly positive $N_\mathbf{k}$ in quadrants I and III and a predominantly negative $N_\mathbf{k}$ in quadrants II and IV, as described in detail in Sec. IV.

The linear dynamics of cyclonic and anticyclonic vortices are identical. The differences evident between graphs (a) and (b) of Figs. 2 and 3 arise from differences in the nonlinear feedback. The simulations we performed confirm this statement.

The energy of the small amplitude anticyclonic vortices decreases (see the graphs for $B=0.1$ and 1.0 in Figs. 2 and 3) due to the negative nonlinear feedback, as is evident in the $N_\mathbf{k}$ field for $B=1.0$ depicted at $t=1.25$ and $t=2.5$ in Figs. 5(a) and 5(b). The energy of the large amplitude anticyclonic vortices increases (see the graphs for $B>2.0$ in Figs. 2 and 3)

due to the positive nonlinear feedback, as is evident in the $N_\mathbf{k}$ field for $B=5.0$ depicted at $t=1.25$ and $t=2.5$ in Figs. 5(c) and 5(d).

The vortex with $B=5$ has the maximum growth rate. For B larger than 5, the grow rate is smaller. For smaller B, the nonlinear interaction cannot redistribute the modes rapidly enough to compensate for the loss of modes in the amplification domains, whereas for larger B, the nonlinear redistribution is so fast that there is not enough time for the modes to experience the transient growth. Therefore for the intermediate value $B=5$, the strongest amplification happens when the conditions for positive nonlinear feedback are satisfied.

The energy of the cyclonic vortices increases initially and then oscillates. This is explained by a sign change of the nonlinear feedback—note the opposite signs of $N_\mathbf{k}$ in the amplification (I and III) and attenuation (II and IV) quadrants for $B=-3.0$ at $t=1.0$ and $t=2.25$ in Figs. 5(e) and 5(f). At
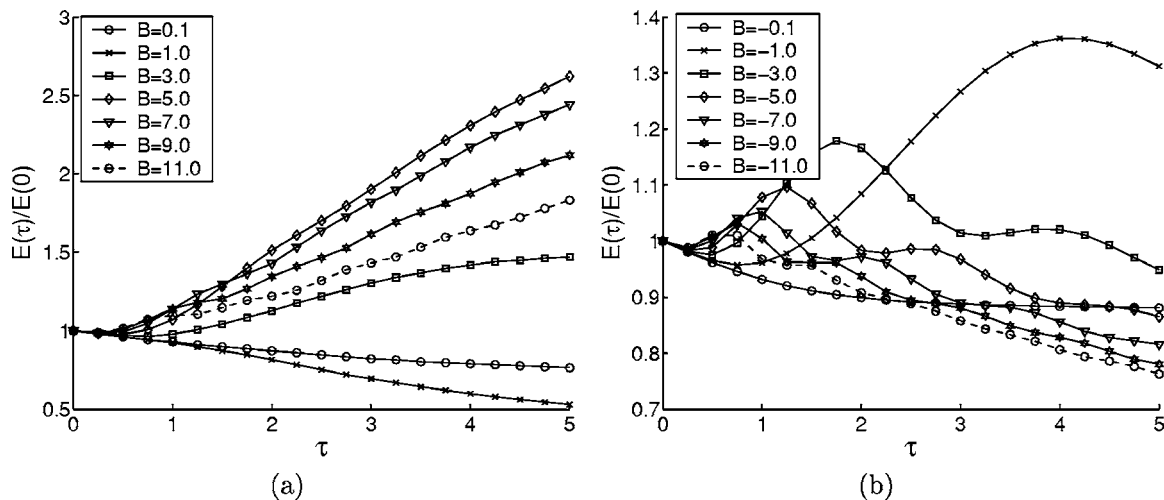

FIG. 3. Time evolutions of (a) anticyclonic and (b) cyclonic perturbation energies at $R_e = 100$ plotted with different B values. The total perturbation energy is normalized by the initial energy.
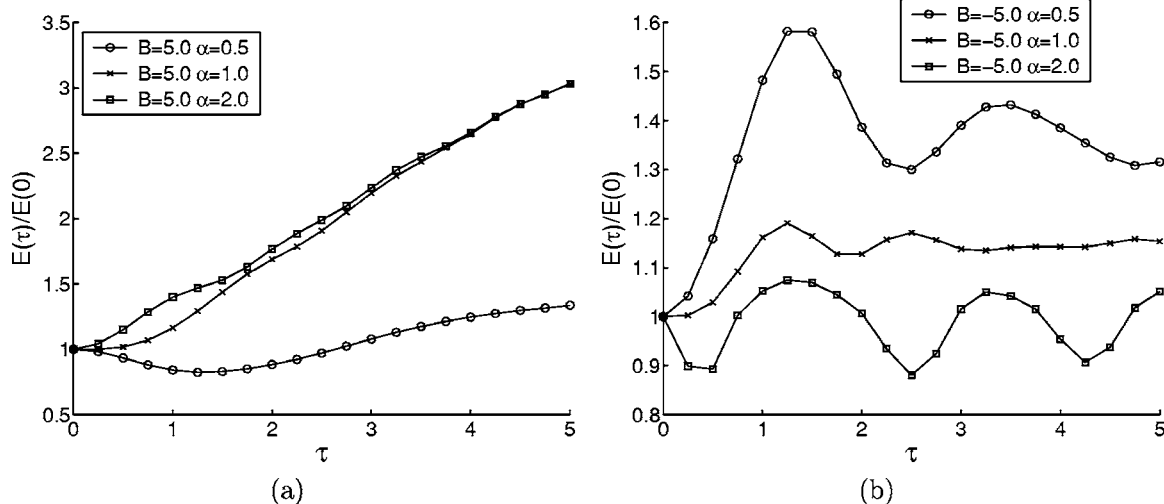
FIG. 4. Time evolution of energy at elliptical (a) anticyclonic and (b) cyclonic vortices. The circular vortex ($\alpha=1$) is $B=\pm5.0$. For $\alpha=1/2$ and 2, the parameters $B=\pm4.472$ are chosen such that the total energies are equal to the energy of a circular vortex with $B=\pm5.0$.

$t=1.0$, N_k is mainly positive in quadrants I and III and is mainly negative in quadrants II and IV. As a result, the total energy is growing at this time. At $t=2.25$ the behavior of N_k is opposite: the total energy is decreasing. As shown in Fig. 3, cyclonic vortices are vulnerable to the viscosity.

The contours of the modal energy E_k (black line contours) and nonlinear energy contribution N_k (density plot, color online only) in Fig. 5 emphasize the anisotropy of the spectral characteristics and physical processes in the **k** plane, in marked contrast to isotropic (Kolmogorov) turbulence.

IV. A QUALITATIVE SKETCH OF THE SELF-SUSTENANCE MECHANISM

The self-sustaining vortex energy observed in Fig. 2(a) (for $B>2.0$) and Fig. 2(b) is the result of a subtle interaction between linear and nonlinear dynamics. Apparently, the balanced interplay is achieved for a limited range of system parameters.

A simple sketch in the (k_X,k_Y) wave number plane is presented in Fig. 6 to explain this interplay. The *active domain* is the region where viscous dissipation is negligible: $k_X^2+k_Y^2<\sqrt{R_e}$. The domain is described by the circle in Fig. 6. The interaction of linear and nonlinear dynamics is described following an individual SFH in the wave number plane.

(i)   A SFH located initially at point 1 in Fig. 6 is in the *amplification domain* of the active domain, where $k_X k_Y>0$. According to process (B), the SFH drifts in the $-k_X$ direction, as indicated by the arrow. The energy of the SFH grows initially.

(ii)   The growth lasts until the wave vector crosses the line $k_Y=0$ at point 2 in Fig. 6.

(iii)   Then, in the *attenuation domain*, where $k_X k_Y<0$, the SFH continues its drift until it reaches point 3, where it is dissipated through viscous friction.

(iv)   Alternatively, the SFH may be relocated to the *amplification domain* by three-wave interaction and the process will repeat.

We present the drift of the SFH only in the right half-plane, as $\Psi(k_X,k_Y)=\Psi^*(-k_X,-k_Y)$. The same process will occur with all of the Fourier harmonics.

If the nonlinear interaction between the Fourier harmonics is inefficient, the perturbation dissipates in the end. A continuous transfer of shear energy to the perturbations is necessary for their long lives. That is possible when the amplification domain (quadrants I and III) is being repopulated through nonlinear interaction (e.g., $\mathbf{k'}+\mathbf{k''}=\mathbf{k}$) between Fourier harmonics that have reached sufficient amplitude. The bypass scenario implies that the dominant transfer of the perturbation energy is from the attenuation domain to the amplification domain, a so-called *positive nonlinear feedback* mechanism.

The long-lived vortex in a shear flow indicates that linear drift and nonlinear interaction are in a positive feedback loop or at least in balance. To what extent the reproduction of the Fourier harmonics in quadrants I and III is sustained, even in the case of positive feedback, depends both on the amplitude and on the spectrum of the initial perturbation. Nonlinear processes are weak at low amplitudes and are not able to compensate for the linear drift of the SFH in the wave number plane. As a result, weak perturbations are damped without any trace and without inducing a transition to turbulence. The higher the amplitude of the initial perturbation, the stronger are the nonlinear effects. At a certain amplitude (which, of course, depends on both the initial vortex perturbation spectrum in the wave number plane and the Reynolds number), the nonlinear processes are able to compensate for the action of the linear drift, thus ensuring the permanent return of the SFH to the amplification areas (quadrants I and III). This eventually ensures the permanent extraction of the energy from the background flow and the maintenance of the perturbations. Hence, the bypass scenario can be realized only in the case of finite amplitude perturbations. In each case it has a threshold that depends on the perturbation spectrum and the Reynolds number.
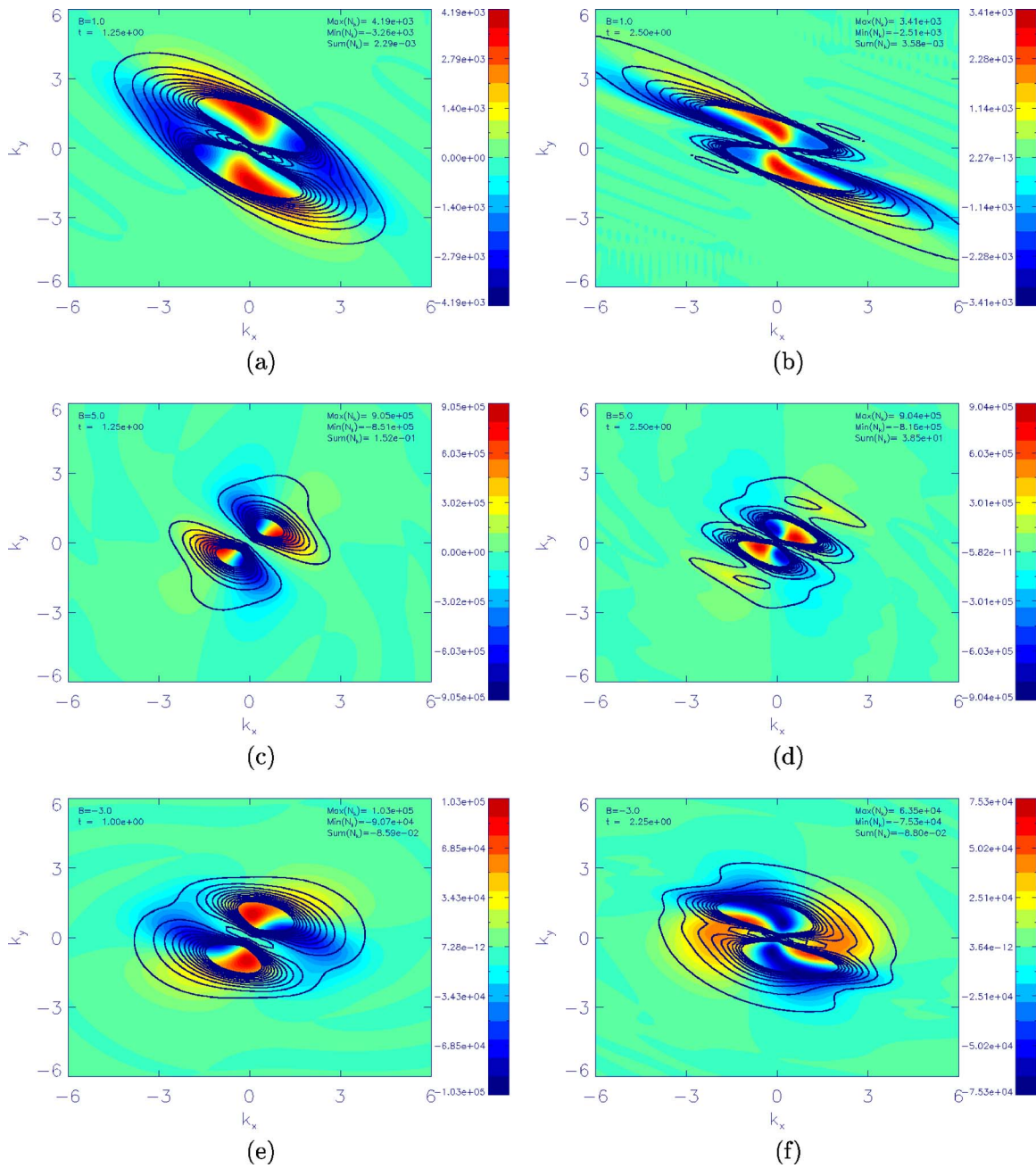
FIG. 5. (Color online) Contours of energy $E_\mathbf{k}$ (line contour) and nonlinear energy contribution $N_\mathbf{k}$ (color density plot) in the k plane. (a) $B=1.0\, t=1.25$; (b) $B=1.0$, $t=2.5$; (c) $B=5.0$, $t=1.25$; (d) $B=5.0$, $t=2.5$; (e) $B=-3.0$, $t=1.0$; and (f) $B=-3.0$, $t=2.25$.

V. APPLICATION TO HASEGAWA-MIMA EQUATION

The electrostatic turbulence of magnetized plasmas within the scale length of ion gyroradius $\rho_s = \sqrt{T_e m_i}/eB$ is described by Hasegawa-Mima (HM) model. The model reduced to

$$\frac{\partial}{\partial \tau}(1-\Delta)\phi - X\frac{\partial}{\partial Y}\Delta\phi - J(\phi, \Delta\phi) + R_e^{-1}\Delta^2\phi = 0, \quad (15)$$

in terms of the electric potential ϕ, the background $\mathbf{E}\times\mathbf{B}$ velocity $\mathbf{V}_{E\times B} = (0, Ax)$, and the energy density

$$E(\tau) = \frac{1}{2}\left[\phi^2 + \left(\frac{\partial\phi}{\partial X}\right)^2 + \left(\frac{\partial\phi}{\partial Y}\right)^2\right]. \quad (16)$$

Here, the dimensionless parameters and variables are rescaled with the vortex size and amplitude as in Sec. II and the density gradient is assumed to be zero.

The apparent differences between the Euler and HM equations are the $\partial\phi/\partial\tau$ term in the dynamics and the corresponding $|\phi|^2$ term in the energy, due to the electron adiabatic response to the electrostatic perturbation.

Figure 7 shows that the HM model behaves almost the same as the Euler model. The total energy of anticyclonic
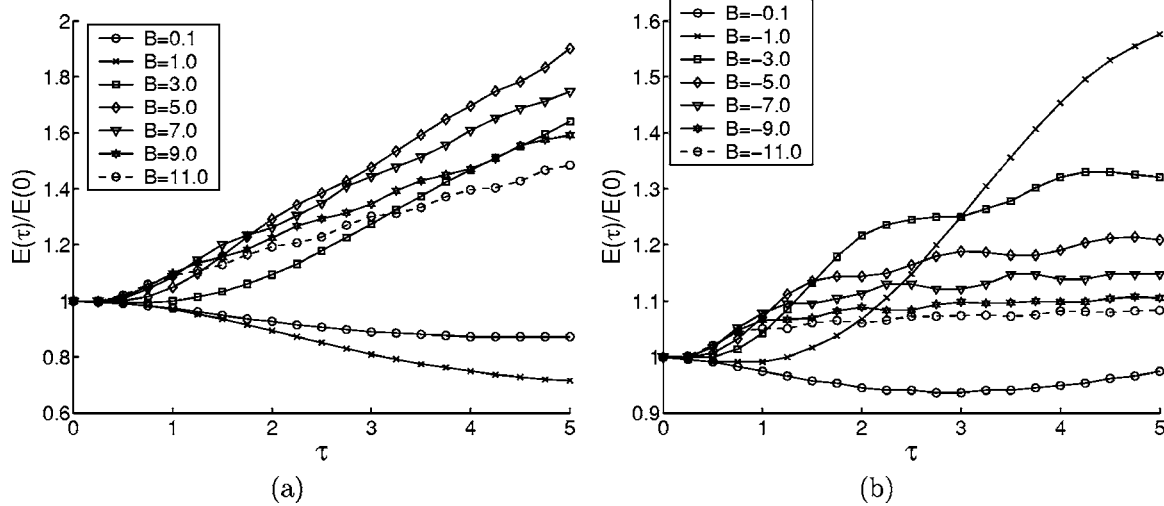
FIG. 6. (Color online) A sketch of the bypass transition applied to planar flow, in the (k_X, k_Y) wave number plane. In the domain $k_X^2 + k_Y^2 < R_e$, viscous dissipation is neglected, where k_X and k_Y are the wave numbers in the flow and shear directions, respectively. The wave number of the SFH drifts from its initial position 1, the SFH is amplified in quadrant I, reaches its maximum amplitude at 2, is attenuated in quadrant II, and undergoes viscous dissipation at 3. The amplification quadrant I is repopulated through nonlinear interaction (e.g., $\mathbf{k}' + \mathbf{k}'' = \mathbf{k}$) from SFHs located in the attenuation quadrants II and IV. (See the text for details.)

vortices increases above approximately $B = 2.0$ and reaches the maximum growth rate at $B = 5.0$, but the maximum slope $\Delta E / \Delta \tau \sim 0.16 E_0$ in energy is relatively smaller than the corresponding slope $0.4 E_0$ in the Euler model. Aside from the nonlinear interaction, anticyclonic vortices, where low-wave-number modes are more dominant due to their immunity to viscous decay, have lower transient growth, $k_X k_Y / (1 + k^2) \approx k_X k_Y \ll k_X k_Y / k^2$, where $k_X, k_Y \ll 1$. The cyclonic vortices show less oscillation in the HM model. In the wave number plane, the slow drift $V_{k_X} = -k^2 k_Y / (1 + k^2) \approx -k^2 k_Y$, where $k \ll 1$, underlies the slow transition of the modes from the amplification region to the attenuation region.
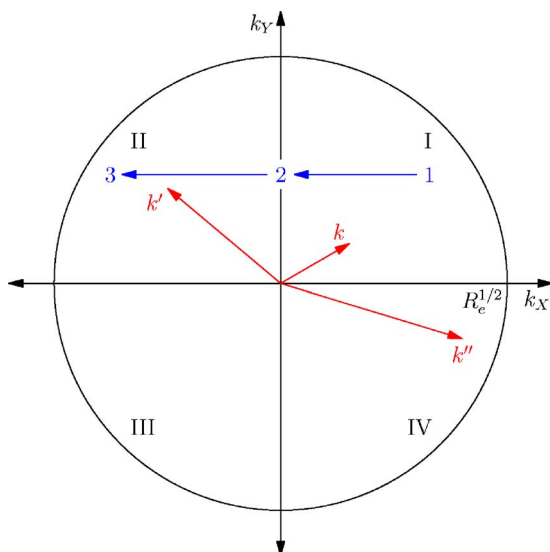

FIG. 7. Time evolutions of (a) anticyclonic and (b) cyclonic perturbation energies at $R_e = \infty$ plotted with different B values with the HM equation. The total perturbation energy is normalized by the initial energy.

VI. PLASMA VORTEX EXPERIMENT

In high-power driven tokamaks, there are several sources of perturbations that arise to seed the formation of vortices. The beam injection lines piercing the magnetic surfaces as well as the RF heating beams break the local symmetry of the magnetic surface which is thought to be a source of local $\mathbf{E} \times \mathbf{B}$ flow generation. The high central power deposition produces sawteeth oscillations which are the finite amplitudes needed to destabilize the neoclassical tearing modes. Tearing modes have convective $\mathbf{E} \times \mathbf{B}$ motions associated with their eigenfunctions. The clearest experimental evidence for the finite amplitude seeds comes from magnetic probes measuring the 1/1 and 3/2 magnetic signals associated with the low mode number m/n resistive magnetohydrodynamic modes. Brennan et al. [17] show an example where 1/1 sawteeth with a recurrence period of 170 ms at significant amplitudes finally destabilizes the damped 3/2 neoclassical tearing mode. Although these magnetic measurements are for relatively large amplitude, low mode number m/n disturbances, driven by the auxiliary heating, we argue that similar small scale drift vortices will be driven by these disturbances. In space plasmas, during magnetic reconnection events in the geomagnetic tail, high speed plasma streams and vortices are created.[18]

In basic laboratory plasma experiments, the mechanism of self-sustenance of vortices by shear flow can be tested. Basic plasma experiments that launch finite amplitude vortex structures and measure their subsequent growth or decay would be of considerable importance for a range of magnetized plasmas. In these experiments with $T_e \simeq 10$ eV, pulsed probes can be used to excite and measure the initial vortices.

In a plasma device, the background electric field is imposed in terms of a bias voltage between a floating cathode and the chamber wall. The imposed electric field forms a background $\mathbf{E} \times \mathbf{B}$ flow. Self-sustaining vortical structures

are observed by controlling a potential profile. The criterion for the self-sustenance of vortices depends on the vortex size and amplitude:

$$B = \frac{e\widetilde{\phi}/T_e}{E_r'\ell^2/(\omega_{ci}\widetilde{B})} \approx 5, \tag{17}$$

in terms of the vortex amplitude $\widetilde{\phi}$, electron temperature T_e, magnetic field $\widetilde{B}$, ion gyrofrequency ω_{ci}, electric field gradient $E_r'=dE_r/dr$, and vortex size $\ell\rho_s$ where ℓ is dimensionless. For example, in a helium plasma with temperature $T_e=10$ eV and magnetic field $B=0.1$ T (for which the scale ρ_s is 0.6 cm and the ion gyrofrequency ω_{ci} is 2.4×10^6 rad/s), the vortical structure with amplitude $e\phi/T_e \sim 0.1$ and radius $10\rho_s \sim 6$ cm needs the voltage $\Delta\phi = 1/2E_r'(l\rho_s)^2 = c_s\rho_s B/100 \approx 0.1$ V across the vortical structure in order to survive for a long time.

To test the lifetime of localized vortices, we propose to use two vorticity probes at the same radius but displaced along **B** in the LAPD experiment.[19] The first probe is used as an antenna to produce cyclonic or anticyclonic vortices and the second probe is used to measure their vorticity with time after launching. The details of the experimental arrangement remain to be fully worked out.

VII. CONCLUSION

In the frame of the two-dimensional Euler equation, we show that a fixed background shear flow can maintain finite amplitude anticyclonic and cyclonic vortices for a long time through a positive feedback mechanism between the nonlinear interactions and the external shearing of the vortex flow. The existence of this positive feedback may indicate a subcritical transition to turbulence. The positive feedback is observed in the simulation, along with self-sustaining vortex perturbations. As optimal growth is expected in three-dimensional flow, the transition to subcritical turbulence will be the next subject of our research. For the simulation of the Hasegawa-Mima equation, we estimated the condition for self-sustaining perturbations. The comparison with plasmas experiments in Helimak or LAPD plasma devices will yield a more controlled understanding of the process.

[1] S. C. Reddy, P. J. Schmid, and D. S. Henningson, SIAM J. Appl. Math. **53**, 15 (1993).
[2] L. Trefethen, A. Trefethen, S. Reddy, and T. Driscoll, Science **261**, 578 (1993).
[3] L. H. Gustavsson, J. Fluid Mech. **224**, 241 (1991).
[4] S. C. Reddy and D. S. Henningson, J. Fluid Mech. **252**, 209 (1993).
[5] K. M. Butler and B. F. Farrell, Phys. Fluids A **4**, 1637 (1992).
[6] J. Baggett, T. Driscoll, and T. L. N., Phys. Fluids **7**, 833 (1995).
[7] T. Gebhardt and S. Grossmann, Phys. Rev. E **50**, 3705 (1994).
[8] B. F. Farrell and P. J. Ioannou, Phys. Fluids A **5**, 1390 (1993).
[9] D. S. Henningson and S. C. Reddy, Phys. Fluids **6**, 1396 (1994).
[10] S. Grossmann, Rev. Mod. Phys. **72**, 603 (2000).
[11] E. Reshotko, Phys. Fluids **13**, 1067 (2001).
[12] S. J. Chapman, J. Fluid Mech. **451**, 35 (2002).
[13] G. Chagelishvili, R. Chanishvili, T. Hristov, and J. Lominadze, JETP **94**, 434 (2002).
[14] A. Hasegawa and K. Mima, Phys. Fluids **21**, 87 (1978).
[15] A. Babiano, C. Basdevant, B. Legras, and R. Sadourny, J. Fluid Mech. **183**, 379 (1987).
[16] W. Horton and A. Hasegawa, Chaos **4**, 227 (1994).
[17] D. P. Brennan, R. J. L. Haye, A. D. Turnbull, M. S. Chu, T. H. Jensen, L. L. Lao, T. C. Luce, P. A. Politzer, E. J. Strait, S. E. Kruger *et al.*, Phys. Plasmas **10**, 1643 (2003).
[18] R. Nakamura, W. Baumjohann, B. Klecker, Y. Bogdanova, A. Balogh, H. Reme, J. M. Bosqued, I. Dandouras, J. A. Sauvaud, K. H. Glassmeier *et al.*, Geophys. Res. Lett. **29**, 1942 (2002).
[19] W. Horton, J. Perez, T. Carter, and R. Bengston, Phys. Plasmas **12**, 022303 (2005).